

TEM Studies and Contact Resistance of Au/Ni/Ti/Ta/n-GaN Ohmic Contacts

D.N. Zakharov¹, Z. Liliental-Weber¹, A. Motayed², and S.N. Mohammad²

¹Lawrence Berkeley National Laboratory, MS 62-203, Berkeley, CA 94720

²Howard University, Electrical Engineering Department 2300 Sixth St. NW, Washington, DC 20059

ABSTRACT

Ohmic Ta/Ti/Ni/Au contacts to n-GaN have been studied using high resolution electron microscopy (HREM), energy dispersive X-ray spectrometry (EDX) and electron energy loss spectrometry (EELS). Two different samples were used: A - annealed at 750⁰C with contact resistance $5 \times 10^{-6} \Omega \text{ cm}^2$ and B – annealed at 775⁰C with contact resistance $6 \times 10^{-5} \Omega \text{ cm}^2$. Both samples revealed extensive in- and out-diffusion between deposited layers with some consumption of GaN layer and formation of $\text{Ti}_x\text{Ta}_{1-x}\text{N}_{50}$ ($0 < x < 25$) at the GaN interface. Almost an order of magnitude difference in contact resistances can be attributed to structure and chemical bonding of Ti-O layers formed on the contact surfaces.

INTRODUCTION

Low resistance ohmic contacts with good thermal stability are necessary for the application of GaN in devices such as light emitting diodes, laser diodes, and heterostructure field effect transistors [1-3]. Significant numbers of investigations have been carried out on ohmic contacts to n-GaN. Among them Ti/Al based metallization system to n-GaN [4,5] and n-AlGaIn/GaN [6,7] were mostly studied. It was shown that TiN formation at the GaN surface is the most important factor for achieving low contact resistivity, since it results in increased donor concentration via N vacancy creation together with the formation of low work function metal [8] at the contact interface. On the other hand with the increase of the annealing temperature Al melts and tends to ball up, most probably forming Al_2O_3 at the contact surface. This causes contact degradation [9,10]. Here we report on Ta-based contacts to n-GaN. Having lower work function than Ti, Ta was deposited to investigate the combined reaction of Ta and Ti with GaN. In order to prevent Ti out-diffusion to the contact surface Ni and Au barrier layers were used. The aim of this work is to study a correlation between the microstructure and contact resistance of ohmic contacts to n-GaN.

EXPERIMENTAL

The GaN films were grown by the metal organic chemical vapor deposition (MOCVD) method on (0001) sapphire substrates. Prior to growth, the substrate was cleaned with hydrogen plasma. An undoped low temperature, 30 nm thick, GaN buffer layer was then deposited on the substrate. Finally, a Si doped ($N_d \sim 5 \times 10^{17} \text{ cm}^{-3}$) GaN epilayer, about 1 μm thick, was grown on the GaN buffer layer. Prior to the metal layers deposition samples were cleaned using a standard procedure. Mesa structures were created by reactive ion etching. Samples were patterned in order to obtain rectangular pads ($250 \mu\text{m} \times 75 \mu\text{m}$) for transmission line measurement (TLM). After photolithography, the samples were immersed into HF: HCl: H_2O (1:1:10) for 15 sec, rinsed in

deionized H₂O and dried. They were loaded immediately for metal deposition. The composite metal layer deposited on n-GaN was Ta/Ti/Ni/Au with the thicknesses of 5nm/50nm/20nm/15nm, respectively. All the metals except Au were deposited by electron beam evaporation. Au was thermally evaporated. Finally, a rapid thermal annealing of the samples was performed in argon gas for 45 sec. at temperatures 750°C for sample A and 775°C for sample B. Contact resistances were derived from the plot of the measured resistance versus gap spacing by TLM. Sample A showed almost one order of magnitude lower contact resistance ($5 \times 10^{-6} \Omega \text{ cm}^2$) with respect to sample B ($6 \times 10^{-5} \Omega \text{ cm}^2$). Further details on the growth process, contact deposition, and TLM measurements can be found in [11].

Samples were studied by transmission electron microscopy (TEM) using a JEOL 3010 and analytical Philips CM200 microscopes operated at 300kV and 200kV, respectively. The latter one was equipped with EDX detector and Gatan imaging filter. Cross-sectional samples for TEM were prepared across contact pads by mechanical polishing down to 10 μm , and further Ar ion milling at 3.5kV until perforation occurred.

RESULTS AND DISCUSSION

Ta/Ti/Ni/Au (5nm/50nm/20nm/15nm) metallization system deposited on n-GaN epilayer, annealed at 750°C and 775°C shows almost one order of magnitude difference in contact resistance $5 \times 10^{-6} \Omega \text{ cm}^2$ (sample A) and $6 \times 10^{-5} \Omega \text{ cm}^2$ (sample B), respectively.

TEM bright field (BF) image (Fig.1a) of the sample A together with energy dispersive X-ray spectrometry (EDX) line profiles (Fig.1b,c) taken across the ohmic contact reveals extensive interdiffusion between deposited layers. Several new layers were formed at the GaN surface after annealing: first Au-Ni layer followed by Ti-Ta, Ni-Ga and Ti-O layers, respectively. The first layer, consisting of Au-Ni crystals, was embedded in the GaN epilayer. As GaN decomposes during the annealing process, the Au-Ni crystals grew in size and merged together to form a pseudo-continuous layer interrupted by GaN material. Pores or V-shaped pits [12] could be observed. These pits were formed at dislocations intersecting the GaN surface (white arrows on Fig.1a). The thickness of the Au-Ni layer can be up to 30nm.

Fig.2a shows a TEM BF image of a contact area. Distribution maps of N, Ti and O in this contact (Figs. 2b, 2c and 2d) were obtained based on electron energy-loss spectrometry (EELS). The concentration of each element is proportional to the intensity in the corresponding image. By comparing images (b) and (c) one can clearly see that Ti and N were present within the previously deposited Ta layer. The thickness of this layer varies between 5nm to 8nm as measured from HREM images. In addition, part of the Ti diffuses to the surface leaving only a thin layer in place of the original Ti layer (Fig.2c). Since oxygen was also present in these two places (Fig.2d), we conclude that Ti-O was formed everywhere except the (Ti,Ta)N layer at the GaN interface. A source of oxygen might be the argon gas used in the annealing process.

HREM image (Fig.3a) clearly demonstrates that Au-Ni crystals are embedded into the GaN epilayer, since the surface of undecomposed GaN is approximately at the same level as the interface between Au-Ni and (Ti,Ta)N (right part of Fig.3a). Fourier transform taken from GaN (Fig.3c) was used to calibrate the HREM image in order to determine d-spacing of lattice fringes observed on Fourier transform taken from Au-Ni/(Ti,Ta)N area (Fig.3b). The error of d-spacing determination is 0.03Å. By analysis of calculated d-spacing and angles between diffraction spots on Fig.3b it is possible to derive that Au-Ni and (Ti,Ta)N compounds both have cubic unit cells with $a_{\text{Au-Ni}}=3.64\text{\AA}$ and $a_{(\text{Ti,Ta})\text{N}}=4.30\text{\AA}$, respectively. The following epitaxial relationships can be

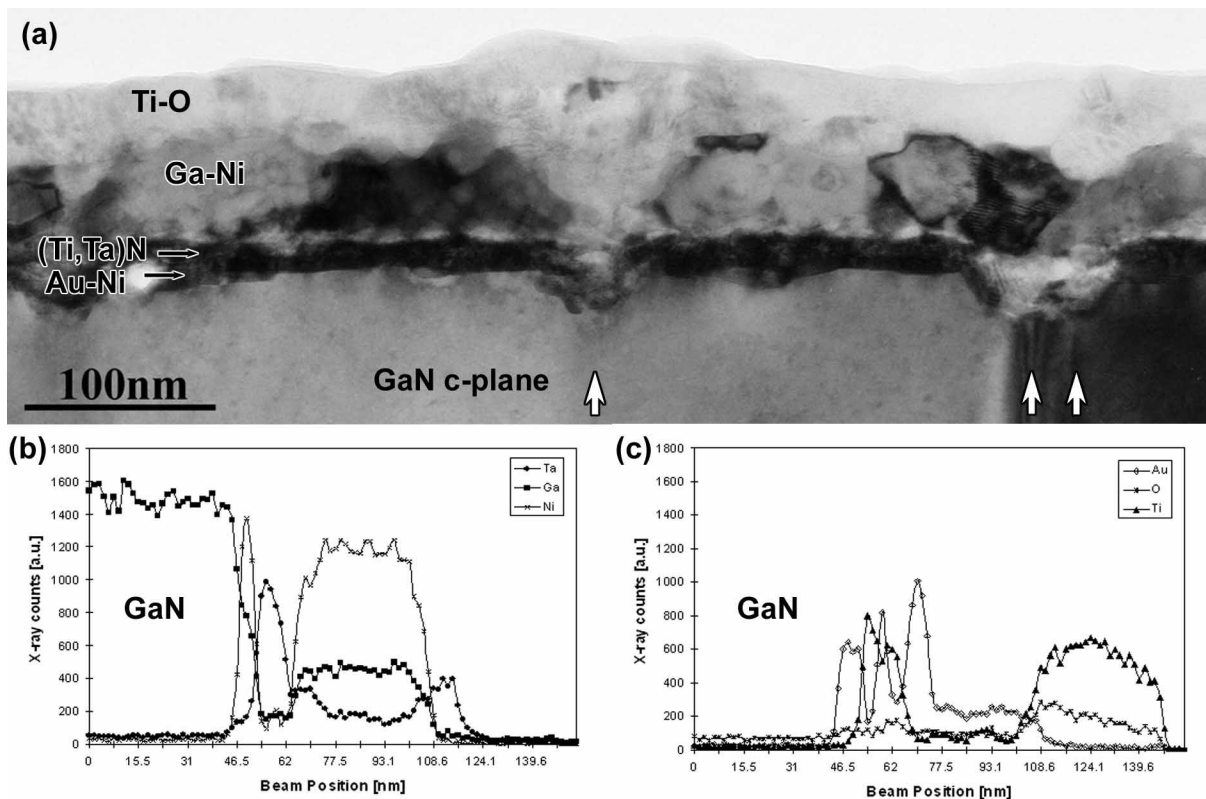


Fig.1. (a) TEM bright field (BF) image of the sample A annealed at 750°C. White arrows show V-shaped pits formed at the dislocation line facing the GaN surface. EDX line profile spectra (b) and (c) show element distribution across the contact.

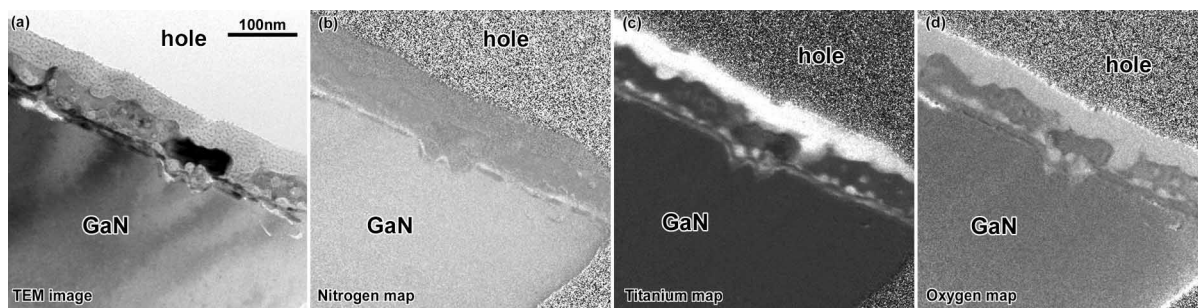


Fig.2. Energy-filtered images (sample A) of a contact area (a) reveal distribution of nitrogen (b), titanium (c) and oxygen (d).

determined: $(111)\text{Au-Ni} \parallel (0002)\text{GaN}$; $[011]\text{Au-Ni} \parallel [2110]\text{GaN}$ and $(111)(\text{Ti,Ta})\text{N} \parallel (0002)\text{GaN}$; $[011](\text{Ti,Ta})\text{N} \parallel [2110]\text{GaN}$.

It is well known that the unit cell parameter in alloys depends on the ratio of the components. Unit cell parameter increases with increase of fraction of atoms having the larger ionic radius. For our case it is possible to conclude that the approximate composition of $\text{Au}_x\text{Ni}_{1-x}$ alloy is between $\text{Au}_8\text{Ni}_{92}$ ($a_{\text{Au}_8\text{Ni}_{92}} = 3.58\text{\AA}$) and $\text{Au}_{50}\text{Ni}_{50}$ ($a_{\text{Au}_{50}\text{Ni}_{50}} = 3.84\text{\AA}$). Similarly, based on values for the TiN and $\text{Ti}_{25}\text{Ta}_{25}\text{N}_{50}$ structures $a_{\text{TiN}} = 4.24\text{\AA}$ and $a_{\text{Ti}_{25}\text{Ta}_{25}\text{N}_{50}} = 4.33\text{\AA}$, one can conclude that $\text{Ti}_x\text{Ta}_{1-x}\text{N}_{50}$, with $0 < x < 25$ was formed. The thickness of the Ti-O layer on the surface of the ohmic contact is between 55nm – 75nm. Structure of this layer will be discussed later in comparison with the sample B.

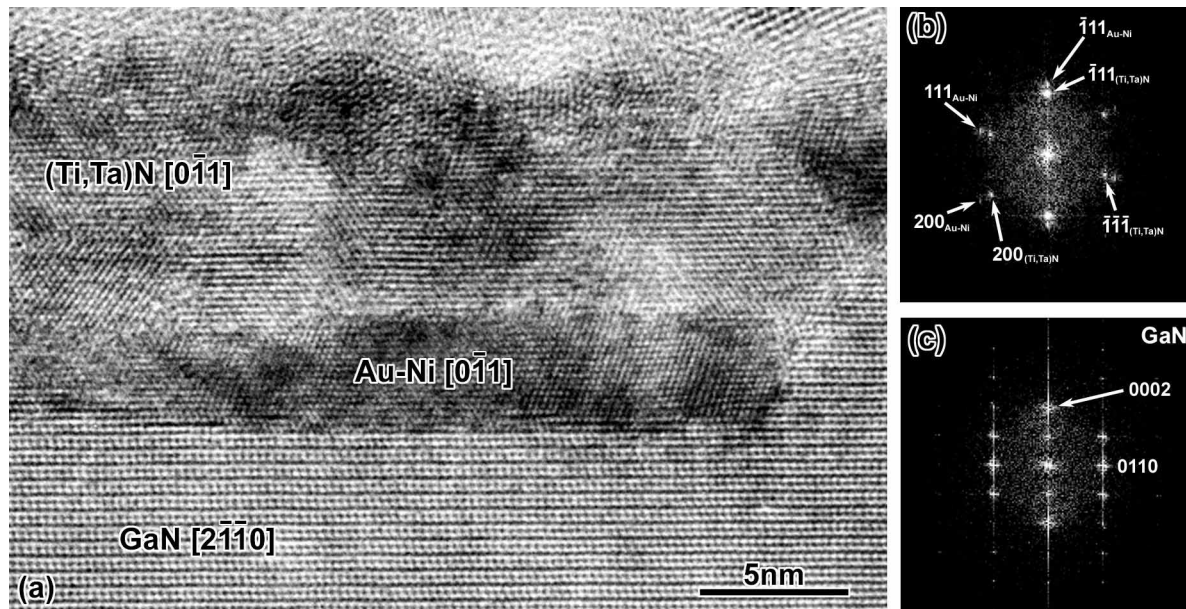


Fig.3. (a) HREM image of an interface between GaN and ohmic contact formed after 750°C annealing (sample A). Fourier transforms from (Ti,Ta)N/Au-Ni (b) and GaN (c) areas allow determination of epitaxial relationships and approximate Ti:Ta and Au:Ni ratios (see text for explanations).

The BF image of sample B and EDX spectra taken across the ohmic contact (Fig.4) reveal formation of four distinct layers. The first one was a pseudo-continuous layer consisting of Au-Ta alloy crystals embedded into GaN. The layer thickness was up to 35nm. Second layer of (Ti,Ta)N with thickness between 5nm to 8nm was formed on the original surface of the GaN epilayer. By analysis of HREM images from the GaN/Au-Ta/(Ti,Ta)N interfaces region it is possible to determine that Au-Ta and (Ti,Ta)N have cubic unit cells with $a_{\text{Au-Ta}}=4.11\text{\AA}$ and $a_{\text{(Ti,Ta)N}}=4.29\text{\AA}$, respectively. This corresponds to $\text{Au}_{90}\text{Ta}_{10}$ and $\text{Ti}_x\text{Ta}_{1-x}\text{N}_{50}$ where $0 < x < 25$. Both layers grow epitaxially on GaN c-plane with epitaxial relationships: $(111)\text{Au}_{90}\text{Ta}_{10} \parallel (0002)\text{GaN}$; $[011]\text{Au}_{90}\text{Ta}_{10} \parallel [2110]\text{GaN}$ and $(111)\text{Ti}_x\text{Ta}_{1-x}\text{N}_{50} \parallel (0002)\text{GaN}$; $[011]\text{Ti}_x\text{Ta}_{1-x}\text{N}_{50} \parallel [2110]\text{GaN}$.

In contrast to sample A where Ni-Ga alloy was observed as a third layer formed on the top of $\text{Ti}_x\text{Ta}_{1-x}\text{N}_{50}$, sample B revealed two typical compositions within the third layer, alternating in lateral dimension. The first one showed on Fig.4a was a polycrystalline ternary Au-Ti-Ta alloy layer with size of crystallites typically in the range of several tens of nanometers. The thickness and lateral dimension of grains with this composition were 60nm-70nm and $2\mu\text{m}$ - $5\mu\text{m}$, respectively. The second type of grains (not shown here) consists of Ni-Ga-Au-Ta alloy with 100nm to 200nm in lateral size. The layer thickness was 60nm-110nm. The lateral size of grains with this composition was usually around $1\mu\text{m}$.

Ti atoms out-diffuse during annealing at 775°C and form titanium oxide on the top of the ohmic contact (Fig.4). The thickness of titanium oxide layer varies between 55nm to 85nm, which is very close to that measured in the sample A. Fig.5 shows EELS spectra of the top Ti-O layer for the sample A and the sample B after 0min, 1min and 6min exposure to the electron beam, respectively. The sample B shows splitting of L_3 and L_2 edges, which suggests that Ti is octahedrally coordinated with oxygen atoms as in TiO_2 [13], whereas in the sample A the splitting is almost negligible. TiO_2 in the sample A is more likely present in relatively low concentrations with respect to sample B and the rest of the oxygen was dissolved in titanium

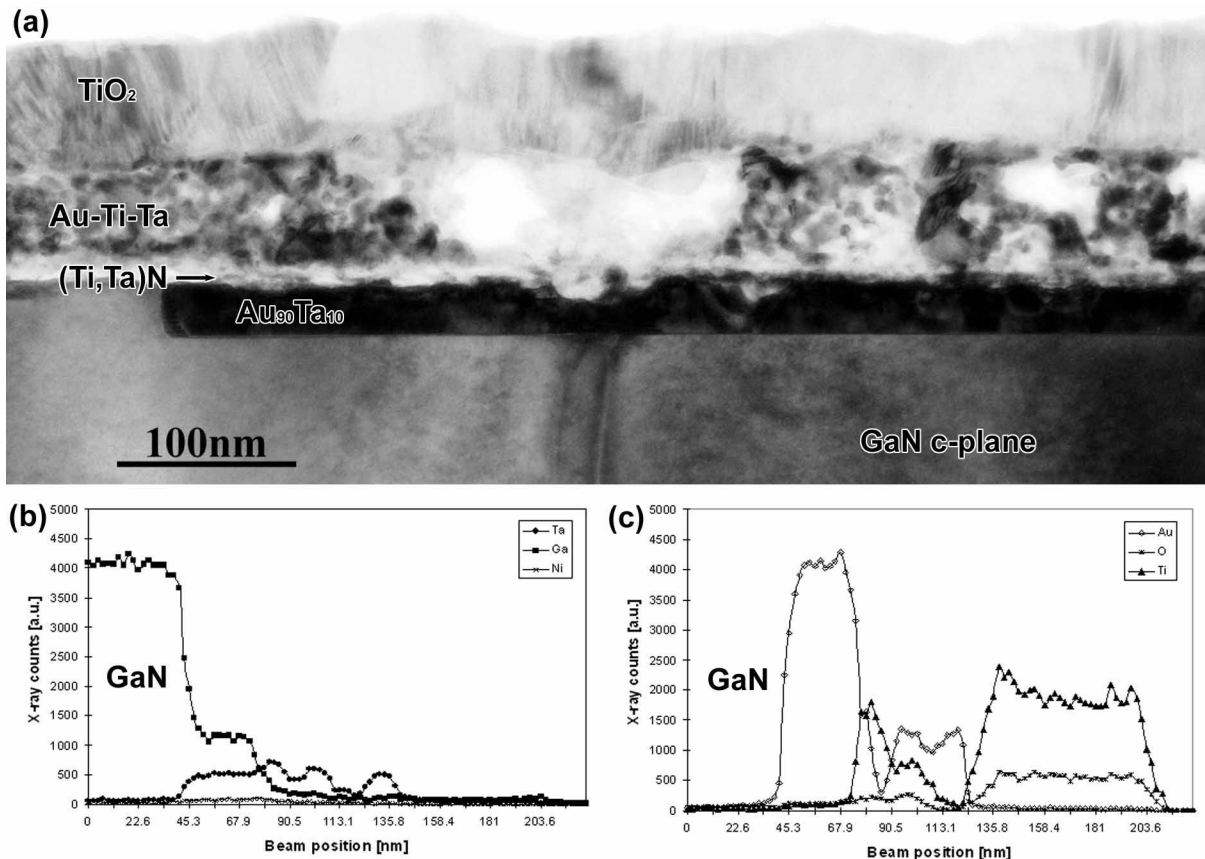


Fig.4. (a) TEM BF image of the sample B annealed at 775°C. EDX line profile spectra (b) and (c) show element distribution across ohmic contact. Note absence of signal from Ni.

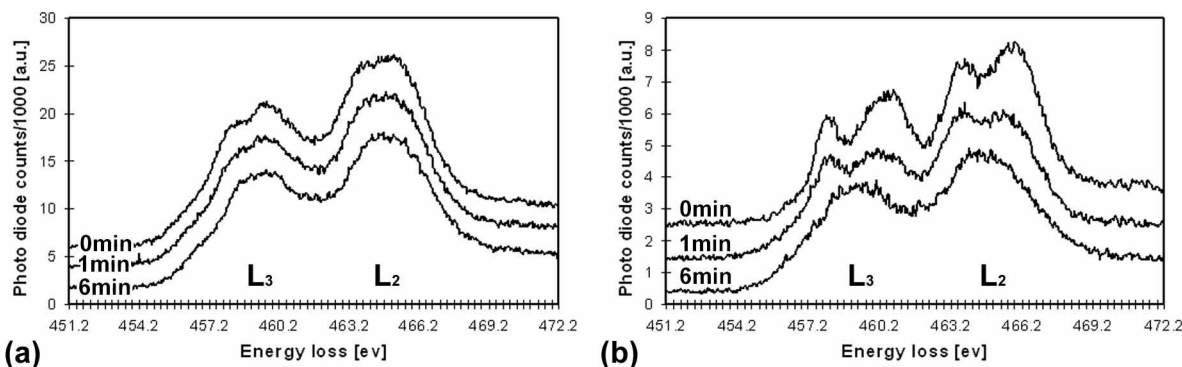


Fig.5. EELS spectra of the Ti-O layer in samples A (a) and B (b) after 0, 1 and 6 minutes exposure to the electron beam respectively.

forming an oxygen reduced TiO_{2-x} phase or Ti-O solution. After illumination by electron beam for 6min both samples revealed the same features in $L_{2,3}$ edges, which could correspond to oxygen reduced titanium oxide.

Finally, both samples revealed diffusion within the metal layers. Au-Ni and $\text{Au}_{90}\text{Ta}_{10}$ pseudo-continuous layers were found embedded into GaN in the samples A and B, respectively. The $\text{Au}_{90}\text{Ta}_{10}$ layer should have a lower Schottky barrier height (due to lower work function of Ta with respect to Ni and Au), and should lower contact resistance in comparison to the Au-Ni.

However, lowering of contact resistance was not observed for higher annealing temperature. Since, a $\text{Ti}_x\text{Ta}_{1-x}\text{N}_{50}$ thin layer, metallic in nature, was formed in both samples at the GaN interface, we believe that formation of a dielectric TiO_2 layer at the contact surface in the sample B is one of the possible reasons for the order of magnitude difference in the samples' contact resistance.

In summary two cross-sectional TEM samples of Ta/Ti/Ni/Au (5nm/50nm/20nm/15nm) deposited on n-GaN and annealed for 45 sec. at 750°C and 775°C have been investigated by TEM methods. Contact layers revealed extensive in- and out-diffusion of metal atoms. Some consumption of the GaN layer and formation of $\text{Ti}_x\text{Ta}_{1-x}\text{N}_{50}$ ($0 < x < 25$) at the GaN interface was observed in both samples. Almost an order of magnitude lower contact resistance measured for the sample A annealed at 750°C can be attributed to structure and chemical bonding differences in the two Ti-O layers formed on the contact surface, as revealed by EELS spectra.

ACKNOWLEDGEMENTS

This work was supported the U.S. Department of Energy under Contract No. DE-AC03-76SF00098 and the Army Research Laboratory Contract No. DAAD17-00-C-0092. The authors would like to thank W. Swider for TEM sample preparation and the National Center for Electron Microscopy at LBNL for the opportunity to use its facilities.

REFERENCES

1. S.N. Mohammad and H. Morkoç, J. Prog. Quantum Electron. **20**, 361 (1996)
2. S. Nakamura, M. Senoh, S.-I. Nagahama, N. Iwasa, T. Yamada, T. Matsushita, H. Kiyoku and Y. Sugimoto, Jp. J. Appl. Phys. Pt.2, **35**, L74 (1996)
3. Y.-F. Wu, B.P. Keller, S. Keller, N.X. Nguyen, M. Le, C. Nguyen, T.J. Jenkins, L.T. Kehias S.P. Denbaars and U.K. Mishra, IEEE Electron Dev. Lett. **18**, 293 (1997)
4. S. Ruvimov, Z. Liliental-Weber, J. Washburn, K.J. Duxstad, E.E. Haller, Z.-F. Fan, S. N. Mohammad, W. Kim, A. E. Botchkarev, and H. Morkoç, Appl. Phys. Lett. **69**, 1556 (1996)
5. L.L. Smith, R.F. Davis, R.-J. Liu, M.J. Kim, and R.W. Carpenter, J. Mater. Res. **14**, 1032 (1999)
6. A.N. Bright, P.J. Thomas, M. Weyland, D.M. Tricker, C.J. Humphreys, and R. Davies, J. Appl. Phys. **89**, 3143 (2001)
7. S.-H. Lim, J. Washburn, Z. Liliental-Weber, D. Qiao, Appl. Phys. Lett. **78**, 3797 (2001)
8. C.A. Dimitriadis, Th. Karakostas, S. Logothetidis, G. Kamarinos, J. Brini, G. Nouet, Solid-State Electronics **43**, 1969 (1999)
9. Z. Fan, S.N. Mohammad, W. Kim, Ö. Aktas, A.E. Botchkarev, and H. Morkoç, Appl. Phys. Lett. **68**, 1672 (1996)
10. Q.Z. Liu and S.S. Lau, Solid-State Electronics **42**, 677 (1998)
11. A. Motayed, R. Bathe, M.C. Wood, O.S. Diouf, R.D. Vispute and S.N. Mohammad, J. Appl. Phys. **93**, 1087 (2003)
12. Z. Liliental-Weber, Y. Chen, S. Ruvimov, and J. Washburn, Phys. Rev. Lett. **79**, 2835 (1997)
13. R. Brydson, L.A.J. Garvie, A.J. Cravent, H. Sauer, F. Hofer and G. Cressey, J. Phys. Condens. Matter. **5**, 9379 (1993)